The Dynamics of the Electric Field Distribution in the Surface of Insulating Film Irradiated by Air Ions

Julionas KALADE [1], Ringaudas RINKUNAS [1]*, Romaldas PURLYS [1], Pranas Juozas ZILINSKAS [1], Tadeus LOZOVSKI [1, 2], Andrius POSKUS [1]

[1] *Faculty of Physics, Vilnius University, Sauletekio 9, LT-10222 Vilnius, Lithuania*

[2] *University of Bialystok, Vilnius Branch, Kalvariju g. 143, LT-03202 Vilnius, Lithuania*

crossref http://dx.doi.org/10.5755/j01.ms.22.1.7132

Received 16 May 2014; accepted 08 November 2014

When deposited on a surface, electric charge usually accumulates near the tips of surface irregularities, from where it can be transferred to nearby objects due to ionization of ambient air. The amount of transferred charge, the rate of charge transfer, the size of the charged spot (e.g., on the surface of an insulator) and its tendency to spread will depend on properties of air during electric discharge, on the magnitude of charge accumulated at the tip of an object, on possibilities for replenishing that charge, on the time spent for charge transfer from the tip onto the insulating layer, on properties of the insulating layer, etc. Those properties are discussed in this work by comparing the results of measurements and theoretical analysis.

Keywords: corona discharge, sheet resistance, ion mobility, conductivity.

1. INTRODUCTION

Ion beams of high intensity can change physical properties of materials [1], stimulate diffusion processes [2], cause ablation [3], local heating [4]. At lower intensities and shorter exposures, the mentioned processes weaken, so that it becomes possible to investigate small-charge effects. Investigations of charge kinetics from a needle-shaped electrode make it possible to determine sheet resistance of an insulator layer [5], charge carrier mobility on the surface of the insulating layer [6], which can depend on properties of adsorbed air [7] or on humidity. Consequently, measurements of humidity can provide useful information when investigating charge carrier mobility [8, 9]. Similarly, if charge carrier mobility depends on radiation intensity, it could be measured, too [9, 10]. Conductivity of air and tangential and normal electric fields created on the insulator surface are determined in this work. Knowledge of those fields is important, because, e.g., when a threshold value of normal electric field is reached, an electric breakdown will occur in the insulator layer and it will be damaged. Knowledge of charge kinetics can be used for estimating the moment of time when charge on the insulating surface must be limited in order to avoid electric breakdown. Tangential electric field strength causes spreading of electric charge over the insulator surface, and if such spreading is impossible due to insufficient conductivity of the insulator, then at sufficiently strong tangential electric fields charge transfer through air can occur (air breakdown).

2. EXPERIMENTAL DETAILS

In this work, it is assumed that electric charge density in the air gap between the needle electrode and the substrate is sufficiently small, so that it does not affect electric fields existing between the needle and the substrate, and it will not be taken into account in the equation describing the electric fields. In addition, collisions of charge carriers with each other and with molecules of the surrounding material are ignored. Since those collisions would cause additional spreading of the charge, the approximation that ignores them only allows determining the smallest possible spreading of charge deposited on an insulator surface.

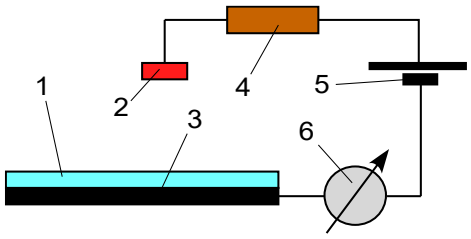

Fig. 1. Experimental setup. 1 – insulator layer (the metallized side is placed upon the metallic substrate 3); 2 – charging needle; 5 – high voltage source with potential U_S; 4 – limiting resistance R; 6 – device for measuring charging current or charge of the insulator layer 1

The investigated system is symmetrical with respect to the needle axis; therefore, cylindrical coordinate system will be used, which in this case has no angular dependence. All quantities only depend on the z coordinate, which is measured in the direction from the needle electrode towards the substrate, and on the polar coordinate ρ (distance to the axis that passes through the needle tip and is normal to the insulator surface). The needle electrode is modeled as a disk with diameter d. The charge that leaves the needle is deposited onto the insulating layer surface, and its surface density is $\sigma(\rho,t)$, where t is time. The charge induced in the substrate is $\sigma_{ind}(\rho,t)$.

* Corresponding author. Tel.: +370-5-2366057; fax: +37052366003.
E-mail address: *ringaudas.rinkunas@ff.vu.lt* (R. Rinkunas)

Fig. 1 shows the setup that was used to measure kinetics of insulator charging current (Fig. 2, curve 4).

In this work, the radius of the needle 2 is $d = 0.2$ mm, the distance between the needle and the insulator layer is $l_1 = 1$ mm, and the dielectric permittivity of ambient air is $\varepsilon_1 = \varepsilon_0$ (it is assumed that relative dielectric permittivity of air is 1). The insulator layer is composed of PET (thickness $l_2 = 40$ μm, dielectric permittivity $\varepsilon_2 = \varepsilon_0 \cdot 3.4$ [11, 12] (ε_0 – electric constant).

The deposited charged spot was developed with an electrophotographic developer using the method of dust chamber.

3. CALCULATION METHOD

The Laplace equation in cylindrical coordinates defines the potential U_1 between the insulator 1 (Fig. 1) surface and the needle electrode 2, and the potential U_2 between the substrate 3 and the insulator surface 1:

$$\begin{aligned} &\frac{\partial^2 U_1(\rho,z,t)}{\partial \rho^2} + \frac{1}{\rho} \times \frac{\partial U_1(\rho,z,t)}{\partial \rho} + \frac{\partial^2 U_1(\rho,z,t)}{\partial z^2} = 0 \\ &\frac{\partial^2 U_2(\rho,z,t)}{\partial \rho^2} + \frac{1}{\rho} \times \frac{\partial U_2(\rho,z,t)}{\partial \rho} + \frac{\partial^2 U_2(\rho,z,t)}{\partial z^2} = 0 \end{aligned} . \quad (1)$$

Solutions of those equations must satisfy the following boundary conditions on the insulator surface at all values of t:

$$\begin{aligned} &U_1\big|_{z=l_1} = U_2\big|_{z=l_1}; \\ &\varepsilon_1 \times \left(\frac{\partial U_1}{\partial z}\right)_{z=l_1} - \varepsilon_2 \times \left(\frac{\partial U_2}{\partial z}\right)_{z=l_1} = \sigma(\rho,t); \end{aligned} \quad (2)$$

and the boundary condition in the substrate:

$$U_2\big|_{z=l_1+l_2} = 0. \quad (3)$$

The current density on the insulator surface is expressed by the equality

$$\vec{j}(\rho,t)\big|_{z=l_1} = \eta \times \vec{E}_z(\rho,t)\big|_{z=l_1}; \quad (4)$$

From Ohm's law, current density j at the needle electrode is

$$\begin{aligned} &j(t)\big|_{z=0} = \frac{U_S - U_{10}(t)}{R \times \pi \times d^2}, \quad \rho \le d \\ &j(t)\big|_{z=0} = 0, \quad \rho > d \end{aligned} , \quad (5)$$

where l_1 is distance between the needle tip and the insulator surface, l_2 is insulator thickness, ε_1 and ε_2 are dielectric permittivities of air and insulator, respectively, R is the resistance that limits the current, $U_{10} = U_1|_{z=00}$ is potential near the needle surface, U_S is the source potential, η is the air conductivity to charge transfer from the needle electrode (this conductivity is assumed to be constant at all points and independent of ρ, z and t). Air conductivity η during the discharge is determined by discharge current, geometry of electrodes participating in the discharge, humidity and composition of ambient air [12]. Consequently, at specific conditions of the experiment, the value of η is not known beforehand (the handbook [12] only allows to estimate the range of possible η values, which is $10^{-8} - 10^{-14}$ $\Omega^{-1} \cdot m^{-1}$). However, by comparing calculated and measured kinetics of current that flows out of the needle, the value of η can be determined with higher precision.

The current density on the insulator surface determines time dependence of the surface charge density $\sigma(\rho,t)$ (this charge density is the same one that appears in Eq. 2):

$$\frac{\partial \sigma}{\partial t} = j(t)\big|_{z=l_1}. \quad (6)$$

The normal component of electric field strength near the surface of the needle is

$$\begin{cases} E_z\big|_{z=0} = \dfrac{U_S - U_{10}}{R \times \pi \times d^2 \times \eta}; \quad \rho \le d; \\ E_z\big|_{z=0} = 0; \quad \rho > d; \end{cases} . \quad (7)$$

Potentials are calculated using the Hankel transform. In order to calculate the current that flows in the external circuit, the time dependence $U_{10}(t)$ must be known (see Eq. 5). This quantity is calculated using the power balance relation.

The component of electric field strength that is normal to the substrate (E_z) and the component that is parallel to the substrate (E_ρ), i.e., tangential, are expressed in terms of corresponding derivatives of the potential:

$$\begin{aligned} &E_z\big|_{z=l_1} = -\left(\frac{\partial U_1}{\partial z}\right)_{z=l_1} \\ &E_\rho\big|_{z=l_1} = -\left(\frac{\partial U_1}{\partial \rho}\right)_{z=l_1} \end{aligned} . \quad (8)$$

As evident from Eq. 5, calculation of current that flows in the external circuit requires knowledge of $U_{10}(t)$ as a function of time. This quantity is estimated using the power balance relation. Let us denote

$$y(t) = \frac{U_{10}(t)}{U_S}. \quad (9)$$

Power created between the substrate 3 (Fig. 1) and needle 2 is expressed as follows:

$$I \times U_{10} = \frac{U_S - U_{10}}{R} \times U_{10} = \frac{U_S^2}{R} \times y \times (1-y), \quad (10)$$

where R is resistance 4 (Fig. 1), I is the total current in the external circuit. On the other hand, the power given by Eq. (10) is equal to the time derivative of energy W released in the mentioned part of the system,

$$W = \frac{1}{2} \times \int U(\rho,t) \times \sigma(\rho,t) \times dS; \quad (11)$$

i.e., to

$$\frac{dW}{dt} = \frac{U_S^2}{R} \times y \times (1-y). \quad (12)$$

In Eq. 11, dS an area element of the surface containing the surface charge $\sigma(\rho,t)$, and $U(\rho,t)$ is the potential on that surface.

Density of charge deposited on the insulator layer is calculated using Eq. 2. The same expression is used to calculate density of charge induced in the metal substrate, but in this case subscript "1" indicates the insulator and subscript "2" indicates the metal, for which $\partial U_z/\partial z = 0$.

4. RESULTS AND DISCUSSION

The current between the needle and the insulator layer begins to flow when electric field between the needle and the layer exceeds the threshold value corresponding to breakdown of the air gap between the needle and the insulator (it has been determined experimentally that when the distance between the needle and the insulator surface is 1 mm, the minimum breakdown voltage is 3500 V).

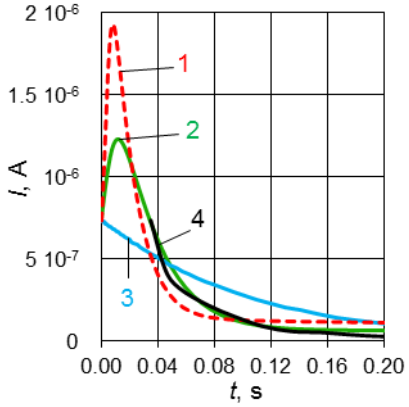

Fig. 2. Current kinetics during discharge from a needle electrode. The limiting resistance is $R = 680$ MΩ. The theoretical curves are calculated using air conductivity: 1 – $\eta = 10^{-9}$ Ω^{-1}·m^{-1}; 2 – $5\cdot10^{-10}$ Ω^{-1}·m^{-1}; 3 – 10^{-10} Ω^{-1}·m^{-1}; 4 – measurement results

As mentioned, calculations have been done neglecting the space charge in the gap between the needle and the insulator. Experimentally, such conditions can be achieved by using the maximum value of limiting resistance, i.e., $R = 680$ MΩ. In this case, by estimating the electrode charge (from an approximate value of electrode capacitance and their potential difference) and the maximum possible current between those electrodes (it would only be limited by the limiting resistance R and by conductivity of air, which is approximately 2 cm^2 V^{-1} s^{-1} [12]), it is possible to estimate the total charge existing between the electrodes. It is approximately equal to half of the charge accumulated in the electrodes. During the current kinetics, the charge between the electrodes can only decrease, because the current decreases, so that the assumption of negligibly small influence of the space charge in the air gap on electric field strength becomes increasingly more justified.

By comparing the calculated current kinetics with experimental ones, it can be seen that theoretical kinetics practically coincide with experimental ones when air conductivity is $5\cdot10^{-10}$ Ω^{-1}·m^{-1}. This value is approximately the same as the value given in the handbook [12]. Thus, it may be concluded that conductivity of air in the region between the needle and the insulator surface during electric discharge can be determined by comparing measured and theoretical current kinetics. The experimental current kinetics coincide with theoretical dependence at all times, which indicates that conductivity of air does not change during the discharge from the needle electrode and is a constant quantity. As evident from Fig. 2, the current does not necessarily decrease in the initial stage of kinetics: in some cases, it may initially increase.

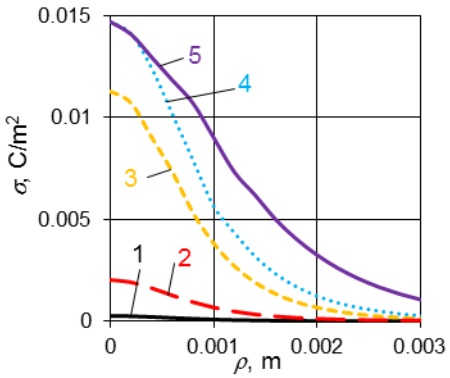

Fig. 3. Distribution of charge deposited on the insulator surface at different moments of time. The limiting resistance is R=680 MΩ. The theoretical curves have been calculated using air conductivity $\eta = 5\cdot10^{-10}$ Ω^{-1}·m^{-1}. Time: 1 – 0.0012 s ; 2 – 0.0075 s ; 3 – 0.046 s ; 4 – 0.273 s ; 5 – 1,635 s

The charge deposited on the insulator layer (Fig. 3) under the tip of the needle is at first large, but after several hundredths or tenths of a second the charge density reaches the maximum value and becomes practically constant. Charge density further away from the needle axis changes with time in a manner consistent with spreading of the deposited charge (as though the charge moves along the insulator surface and this causes spreading of the charged spot), but this apparent "spreading" of charge is actually a result of redistribution of electric fields between the needle and the insulator surface. The latter "spreading" of charge can be as long as several tens of minutes and is caused by decrease of normal electric field strength E_z and increase of tangential electric field strength E_ρ with time near the insulator surface, so that the moving charge carriers are increasingly deflected away from the needle axis. Such "spreading" is also characteristic of the charge induced in the substrate and the tangential electric field strength. The theoretical calculations have been done assuming that charge carriers are immobile on the insulating layer surface.

The charge induced in the metal substrate at different moments of time is shown in Fig. 4. Initially, that charge is only determined by the charge accumulated in the needle. As charge is transferred from the needle onto the insulator surface, the charge existing both in the needle and the metal substrate increases and spreads. The difference in Fig. 3 and Fig. 4 is only in the initial time moments.

The deposited and induced charges defines the electric field strength in the isolator. Too great fields strength can breakdown the isolator material. The tangential electric field strength E_ρ on the insulator surface can cause drift of deposited charge carriers. Distributions of tangential electric field strength at different times are shown in Fig. 5. We see that tangential field strength is equal to zero just below the needle. From the theoretical expression of E_ρ it follows that $E_\rho \sim \rho$ when $\rho \to 0$. When $\rho \to 0$, the divergence of drift current, which determines time variation of charge density, is proportional to $\left(\frac{1}{\rho}\times\frac{\partial}{\partial\rho}(\rho\times E_\rho)\right)_{\rho\to0} \neq 0$.

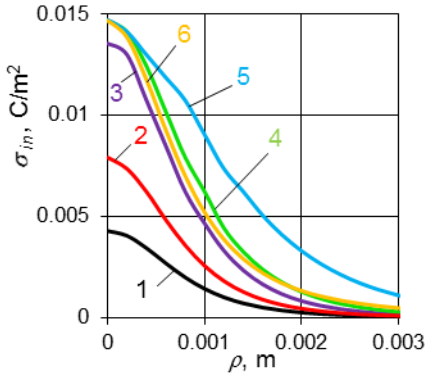

Fig. 4. Distribution of charge induced in the metal substrate at different moments of time. The limiting resistance is R=680 MΩ. The theoretical curves were calculated using air conductivity η=5·10^{-10} Ω^{-1}·m^{-1}. Time: 1 – 0.0012 s; 2 – 0.0075 s; 3 – 0.046 s; 4 – 0.273 s; 5 – 1.635 s. Curve 6 was obtained by calculating the induced charge in the substrate using the transform theory

Thus, charge carrier drift is one of the reasons why carriers can leave the point $\rho = 0$. Unlike the tangential electric field on the surface of the metal substrate, the tangential electric field on the insulator surface can be non-zero even at the initial moment of time (depending on geometry of the system), when there is no charge deposited on the insulator surface. The distribution of tangential electric field was also calculated for the case when the needle is removed after depositing charge on the insulator surface. The results indicate that in this case the tangential electric field stays practically the same. Distributions of deposited charge density, induced charge density and normal electric field are also unchanged.

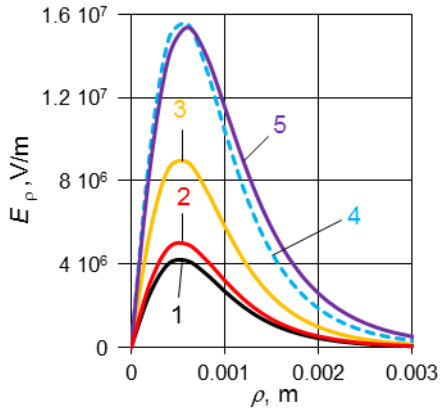

Fig. 5. Distributions of tangential electric field strength on the insulator surface at different moments of time. The limiting resistance is R = 680 MΩ. The theoretical curves have been calculated using air conductivity η = 5·10^{-10} Ω^{-1}·m^{-1}. Time: 1 – 0 s; 2 – 0.0012 s; 3 – 0.0075 s; 4 – 0.046 s; 5 – 0.273 s. This field can cause drift of charge carriers existing on the insulator surface

Distributions of normal electric field strength at different times are shown in Fig. 6. The normal electric field strength determines the energy of a charge carrier when it collides with the insulator surface. That energy determines the probability that a molecule existing on the insulator surface (e.g., a water molecule) escapes from the surface after the collision. If binding energy of those molecules is less than energy of incident ions, then those molecules will escape. In addition, charge carriers can collide not only with neutral molecules, but also with ions that were deposited earlier, and thus stimulate motion of those ions on the insulator surface (as a result, ions would spread almost uniformly inside a certain oval area). At first, the normal field strength increases with time, but later on it starts to decrease and approaches zero, whereas the charge deposited on the insulator surface becomes almost equal to the charge induced in the substrate.

The charge deposited on the insulator surface (Fig. 3) can be developed with an electrographic developer and thus it can be ascertained if theoretical estimates of charge spread are in accord with experimental results. The results of measurements indicate that electrographic developer only allows developing potentials down to several volts (lower potentials are not developed).

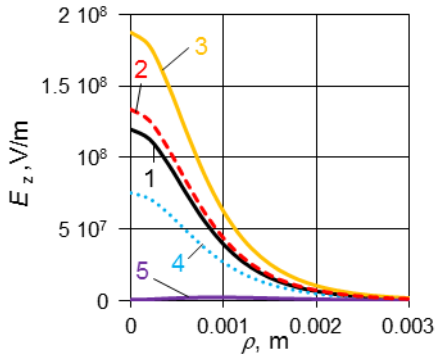

Fig. 6. Distributions of normal electric field strength on the insulator surface at different moments of time. The limiting resistance is R = 680 MΩ. The theoretical curves have been calculated using air conductivity η = 5·10^{-10} Ω^{-1}·m^{-1}. Time: 1 – 0 s; 2 – 0.0012 s; 3 – 0.0075 s; 4 – 0.046 s; 5 – 0.273 s. The normal electric field strength determines the energy of the incident charge carrier when it collides with the insulator surface

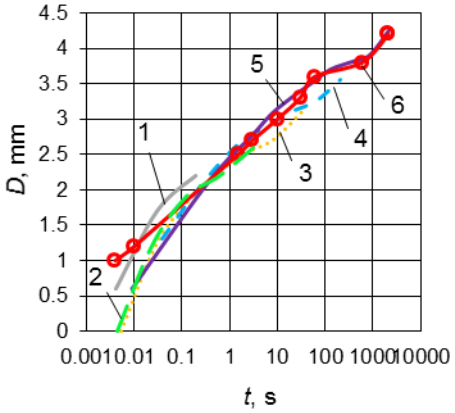

Fig. 7. Time dependence of diameter D of the charged spot on the insulator surface, developed with an electrographic developer. The limiting resistance is R = 680 MΩ. The theoretical curves were calculated using the following air conductivity: 1 – η = 10^{-9} Ω^{-1}·m^{-1}; 2 – 10^{-10} Ω^{-1}·m^{-1}; 3 – 10^{-11} Ω^{-1}·m^{-1}; 4 – 10^{-12} Ω^{-1}·m^{-1}; 5 – 10^{-13} Ω^{-1}·m^{-1}; the diameter D is defined as the diameter of the area where charge density exceeds 10^{-3} C/m^2; experimental results are given by curve 6. Air conductivity has practically no effect on the size of the charged spot

Consequently, the charge density corresponding to such potential values has been used as the minimal charge density that can be developed with an electrographic developer. Using this quantity, the theoretical value of the

radius of the charged spot has been calculated. That radius has been calculated for various values of air conductivity. The results are shown in Fig. 7.

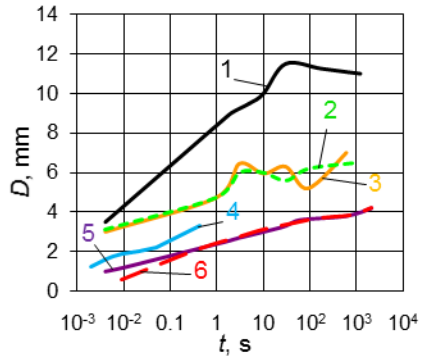

Fig. 8. Time dependence of the size of the charged spot on the insulator surface, developed with an electrographic developer: 1 – the measured dependence when R = 790 kΩ; 2 – when R = 7.3 MΩ; 3 – when R = 60 MΩ; 4 – the calculated dependence when R = 60 MΩ and $\eta = 2 \cdot 10^{-9}$ $\Omega^{-1} \cdot m^{-1}$; 5 – the measured dependence when R = 680 MΩ; 6 – the calculated dependence when R = 680 MΩ and $\eta = 5 \cdot 10^{-10}$ $\Omega^{-1} \cdot m^{-1}$

As evident in Fig. 7, conductivity of air has practically no influence on spreading of the charged spot during charge deposition on the insulator surface (one should keep in mind that charge carriers on the insulator surface are immobile). An increase of air conductivity causes an increase of current density and thus an increase of charge carrier concentration. For measuring the diameter of the charged spot, each point of the time dependence (Fig. 7, curve 6) was determined by allowing the current to flow until time t. Then, the current flow was interrupted and the diameter of the charged spot was measured by developing the deposited charge with an electrographic developer. A good agreement between experiment and theory indicates that charge carriers do not move on the insulator surface and that the charge carriers that move between the needle and the insulator surface have no significant influence on electric field between the needle and the metal substrate. The distribution of the deposited charge is determined by geometry of the system.

Fig. 7 can be used to determine conditions when theoretical results are sufficiently accurate (i.e., when the charge existing between the needle and the insulator surface does not affect the distribution of electric field). As evident from Fig. 7, when R = 680 MΩ, the calculated size of the charged spot does not depend on air conductivity. Fig. 8 shows time dependence of the radius of the developed charged spot at various values of the limiting resistance R. At R = 790 kΩ and R = 7.3 MΩ, the theoretical current kinetics are very different from experimental ones (Fig. 2). Consequently, at those values of the limiting resistance, the theoretical model described in this work is not suitable. If R is increased to 60 MΩ, the calculated current kinetics become more similar to experimental ones (Fig. 9).

However, in this case the initial part of the experimental current kinetics coincides with the theoretical curve corresponding to air conductivity $5 \cdot 10^{-9}$ $\Omega^{-1} \cdot m^{-1}$ (the experimental curve may be shifted along the time axis, because at the time when measurement of that curve starts, the current is not zero, and its initial value is determined by the chosen magnitude of the synchronization pulse), whereas the final part of the experimental current kinetics coincides with the theoretical curve corresponding to air conductivity $2 \cdot 10^{-9}$ $\Omega^{-1} \cdot m^{-1}$.

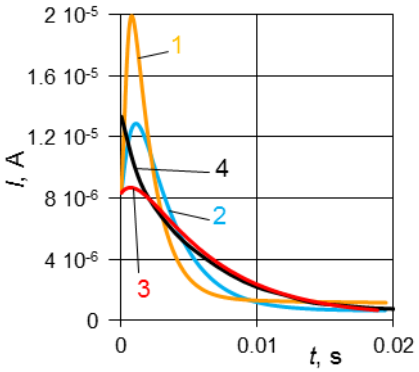

Fig. 9. Kinetics of current during discharge from a needle. The limiting resistance is R = 60 MΩ; y_0 = 0.875. The theoretical curves have been calculated at air conductivity: 1 – $\eta = 10^{-8}$ $\Omega^{-1} \cdot m^{-1}$; 2 – $5 \cdot 10^{-9}$ $\Omega^{-1} \cdot m^{-1}$; 3 – $2 \cdot 10^{-9}$ $\Omega^{-1} \cdot m^{-1}$; 4 – experimental results

It follows that η is not constant. Instead, η depends on current and thus varies with time (it means that the expression of current density given by Eq. 4, where η = const, is not suitable and must be modified by replacing η with an accurate expression: e x μ x η, where μ is ion mobility and n is ion density. However, this would greatly complicate calculations of electric field strength and magnitude of deposited charge). In addition, the calculated spread of the charged spot is less than the measured one. This discrepancy could be caused by motion of deposited charge along the insulator surface, which is neglected in the theoretical model.

The total electric field strength inside the insulator is important for investigations of insulator properties. For example, it is needed in order to determine if electric breakdown will occur at a particular value of electric field, or if charge carrier transfer caused by high electric field [13] will occur (e.g., hopping or tunneling of charge carrier between localization states), etc. Calculations indicate that the total electric field inside the insulator is initially largest near the substrate, and it becomes larger as the charge is being deposited. The normal and total electric fields inside the insulator near its free surface also increase during deposition of charge. The electric field is strongest at the point ρ = 0. Consequently, the insulator breakdown is most likely to start at that point (in the case of PET, the breakdown electric field strength is $2 \cdot 10^7$ V/m [12]). The maximum electric field created inside the insulator is normal to the insulator surface, and its magnitude is determined by the charge deposited on the insulator surface. As the deposited charge is increased, the total electric field becomes increasingly parallel to the normal of the insulator surface at every point of the insulator. The calculation results can be used to determine ranges of values of system parameters (air gap width, insulator thickness, its relative dielectric permittivity, etc.) that correspond to absence of breakdown or which values of electric field strength are small enough to maintain integrity of the insulator, but at the same time large enough to cause charge carrier transfer phenomena.

During charge deposition on the insulator surface, the normal component of electric field in air at first increases (Fig. 6), but later on it starts to decrease and approaches zero at the point just below the needle. The field only remains non-zero further from the center of the needle. Thus, if it were possible for additional charge carriers to be transferred from the needle onto the insulator surface, then that field would direct them away from the needle axis, and this would make the charged spot to spread on the insulator surface. However, when electric field strength just below the needle drops to zero, the needle is "closed" (Eq. 5).

The electrical breakdown occurs near needle tip. So we can expect and calculations show this, that only negligible influence of insulator electrical permittivity and insulator thickness on electrical breakdown can be seen. Insulator surface in this work was considered as perfectly flat.

4. CONCLUSIONS

The technique described in this work can be used to measure air conductivity during discharge.

Deposited on the insulator surface charge spread is a result of redistribution of electric fields between the needle and the insulator surface.

The results of this work can be used to calculate magnitude of electric fields formed by deposition of charge on the insulator and thus to find out if those fields will not exceed the threshold value of air breakdown on insulator surface. Also an electric field strength in the insulator can be determined, which cause a breakdown or stimulate charge transfer phenomena in insulator material. Experimental system parameters can be selected for desired result.

The rate of charge transfer is not a determining factor for distributions of charge density and electric field strength on the insulator surface, the main factor is the total charge that has left the needle.

REFERENCES

1. **Twardowski, A., Makowski, P., Małachowski, A., Hrynyk, R., Pietrowski, P., Tyczkowski, J.** Plasma Treatment of Thermoactive Membrane Textiles for Superhydrophobicity *Materials Science (Medžiagotyra)* 18 (2) 2012: pp. 163 – 166.
2. **Galdikas, A., Petraitienė, A.** Modeling of Nitrogen Penetration in Medical Grade CoCrMo Alloy during Plasma Nitriding *Materials Science (Medžiagotyra)* 20 (1) 2014: pp. 25 – 29. http://dx.doi.org/10.5755/j01.ms.20.1.3458
3. **Levinskas, R., Kezelis, R., Brinkiene, K., Grigaitiene, V., Valincius, V., Lukosiute, I., Kavaliauskas, Z., Baltusnikas, A.** High Temperature Ablation of Composite Material under Plasma Jet Impact *Materials Science (Medžiagotyra)* 17 (4) 2011: pp. 423 – 427. http://dx.doi.org/10.5755/j01.ms.17.4.781
4. **Alontseva, D., Pogrebnjak, A., Kolesnikova, T., Russakova, A.** Modeling of Processes in Co-Based Coatings Exposed to Plasma Jet Irradiation *Materials Science (Medžiagotyra)* 19 (3) 2013: pp. 277 – 282.
5. **Kim, K., Zhao, Y., Jang, H., Lee, S., Kim, J., Kim, K., Ahn, J., Kim, P., Choi, J., Hong, B.** Large-scale Pattern Growth of Graphene Films for Stretchable Transparent Electrodes *Nature* 457 (5) 2009: pp. 706 – 710.
6. **Sholl, D.** Understanding Macroscopic Diffusion of Adsorbed Molecules in Crystalline Nanoporous Materials via Atomistic Simulations *Accounts of Chemical Research* 39 2006: pp. 403 – 411. http://dx.doi.org/10.1021/ar0402199
7. **Barsan, N., Hubner, M., Weimar, U.** Conduction Mechanisms in SnO_2 Based Polycrystalline Thick Film Gas Sensors Exposed to CO and H_2 in Different Oxygen Backgrounds *Sensors and Actuators* B 157 2011: pp. 510 – 517.
8. **Tanga, Q., Chan, Y., Zhang, K.** Fast Response Resistive Humidity Sensitivity of Polyimide/multiwall Carbon Nanotube Composite Films *Sensors and Actuators* B152 2011: pp. 99 – 106. http://dx.doi.org/10.1016/j.snb.2010.09.016
9. **Rinkunas, R, Kuskevicius, S.** A Contactless Method of Resistance Measurement *Technical Physics* 59 (1) 2009: pp. 133 – 137.
10. **Duffo, G., Arva, E., Schulz, F., Vazquez, D.** Durability of a Reinforced Concrete Designed for the Construction of an Intermediate-level Radioactive Waste Disposal Facility *Journal of Nuclear Materials* 420 2012: pp. 382 – 387.
11. **Drake, G.W.F.** Handbook of Atomic, Molecular and Optical Physics, Springer, Berlin, 2006: pp. 1342. http://dx.doi.org/10.1007/978-0-387-26308-3
12. **Kikoin, I.K.** Tables of Physical Unities, Atomizdat, Moscow (in Russian), 1976: pp. 1007.
13. **Hadri, B., Mamy, P.R., Martinez, J., Mostefa, M.** Electrical Conduction in a Semicrystalline Polyethylene Terephthalate in High Electric Field *Solid State Communications* 139 2006: pp. 35 – 39.